



Crack initiation stress of brittle rock with different porosities

Minghao Tang¹ · Guibin Wang² · Shiwan Chen³ · Chunhe Yang^{1,2}

Received: 3 October 2020 / Accepted: 6 March 2021 / Published online: 23 April 2021
© Springer-Verlag GmbH Germany, part of Springer Nature 2021

Abstract

Accurately determining the crack initiation stress (CI) is of great importance to evaluate the stability of deep underground openings and the permeability of host rock in the near field. For this paper, uniaxial compression tests and increasing amplitude cyclic stressing tests were performed on four kinds of rocks with different porosities. The stress-strain data and acoustic emission (AE) data of these tests are analyzed to evaluate the applicability and accuracy of the existing methods for determining the CI. The results demonstrate that for marble and Beishan granite with low porosity, the lateral strain (LS) method is the simplest and most direct method to obtain the CI_{LS} . For high porosity sandstone, the result of lateral strain response (LSR) method is significantly smaller than that obtained by AE. The cumulative AE hits (CAEH) method heavily depends on the “S-shaped” characteristic of the cumulative AE hits curve, which limits its scope of application. The cumulative AE hits curve slope (CAHS) method, which determines the key inflection point of the cumulative AE hits curve by slope variation to determine the CI_{CAHS} , possesses the widest applicability and highest accuracy. The CI/UCS ratios of rocks with similar grain sizes decreases with increasing porosity. For Beishan granite, the average CI_{CAHS} is less than that of CI_{LS} . They are 0.43 UCS and 0.53 UCS, respectively. According to the residual strain data from the cyclic loading tests, the two crack initiation thresholds of Beishan granite can be clearly identified. These two crack initiation thresholds represent different crack initiation sequences in grain boundaries and different minerals.

Keywords Crack initiation stress · Lateral strain · Brittle rocks · Lateral strain response · Cyclic stressing · Acoustic emissions

Introduction

The deformation and failure before the peak strength of rock include four stages: crack closure stage, elastic stage, stable crack growth stage, and unstable crack growth stage (Brace et al. 1966; Martin and Chandler 1994; Eberhardt et al. 1998; Diederichs et al. 2004; Cai et al. 2004). These four stages can be divided by three key stress thresholds, including the crack closure stress (CC), the crack initiation stress (CI), and the

crack damage stress (CD). The in situ failure strength of deep tunnels in brittle rock does not match the compressive strength determined in laboratory tests. Fairhurst and Cook (1966) evaluated thin spalling along the maximum compressive stress observed around deep South African tunnels. Martin et al. (1999) observed that spalling would occur when the maximum tangential stress exceeded approximately 0.4 times the uniaxial compressive strength (UCS) in a square tunnel in South Africa. Diederichs (2007) proposed that the CI be taken as the lower bound of in situ spalling strength and established the damage initiation and spalling limit (DISL) method. This criterion was also applied to the hazard analysis and the depth of failure prediction of tunnels with complicated geometry. It was also suggested by Martin and Christiansson (2009) and Andersson et al. (2009) that the CI obtained from uniaxial compression tests can be used as an estimate of the in situ spalling strength. In the construction of a high-level waste disposal repository, accurate prediction of the depth of failure around excavations is of great significance to evaluate the long-term stability of the repository and to reduce the radionuclide migration pathways (Wang et al. 2018). Therefore, the

✉ Guibin Wang
gbwang@whrsm.ac.cn

¹ State Key Laboratory of Coal Mine Disaster Dynamics and Control, School of Resources and Safety Engineering, Chongqing University, 400044 Chongqing, China

² State Key Laboratory of Geomechanics and Geotechnical Engineering, Institute of Rock and Soil Mechanics, Chinese Academy of Sciences, Wuhan 430071, Hubei, China

³ College of Resources and Environment Engineering, Guizhou University, Guiyang 550025, Guizhou, China

development of a reliable method to determine the CI for uniaxial compression test has been a research focus for scholars.

In the past few decades, many methods based on stress-strain analyses and acoustic emission data have been put forward to determine the CI, such as the volumetric strain method (Brace et al. 1966), the lateral strain method (Lajtai 1974), the crack volumetric strain (CVS) method, the instantaneous Poisson's ratio method (Diederichs 2007), the lateral strain response (LSR) method (Nicksiar and Martin 2012), the cumulative AE hits (CAEH) method (Zhao et al. 2013, 2015), and the relative compression strain response (RCSR) method (Wen et al. 2018). For the volumetric strain method, the lateral strain method, and the instantaneous Poisson's ratio method, the rock samples after crack closure are regarded as the elastic material, and the CI is determined by defining the onset of the deviation of the curve from linearity. However, there is no real linear stage in the whole deformation process when many pre-existing flaws are present in the sample. Eberhardt et al. (1998) indicated that the CVS method depended on the accurate determination of elastic parameters. Zhao et al. (2015) demonstrated that the CI determined by LSR method had a strong correlation with the CD. Meanwhile, the applicability of LSR method and CAEH method for other lithological rocks also remains to be verified.

Porosity represents the bulk void space in rock, mainly including fissures, pores, and open cracks, which play a role in stress concentration (Palchik and Hatzor 2002; Chen et al. 2021). Basu and Mishra (2014) proposed that the effective porosity can be used to estimate the CI and uniaxial compressive strength. In general, the CI/UCS is negatively correlated with porosity and average particle size (Hatzor and Palchik 1997; Nicksiar and Martin 2013). Brace et al. (1966) determined a normalized value of CI to peak stress of 0.50 for granite, 0.45 for marble, and 0.45 for aplite. Nicksiar and Martin (2013) collected a large amount of data for igneous rocks, sedimentary rocks, and metamorphic rocks and found that the average CI/UCS ratios were 0.458, 0.463, and 0.468 when obtained by the LSR method. Peng et al. (2018) used the CVS method to obtain the average CI/UCS ratios of igneous rocks, sedimentary rocks, and metamorphic rocks from 926 sets of data as 0.503, 0.402, and 0.473, respectively. Similarly, 227 sets of igneous rocks, sedimentary rocks, and metamorphic rocks were collected, and the average CI/UCS ratios obtained by the RCSR method were 0.503, 0.3759, and 0.5396, respectively. Taheri et al. (2020) determined the CI of different types of rocks by identifying transition points and evaluated the accuracy of these methods by standard deviation. These researchers used a large amount of data to prove that the results obtained by various methods are statistically acceptable. However, focusing solely on statistical

correctness may mask the shortcomings of these methods. When the amount of data is small, the blind use of a certain method may cause large errors.

This paper evaluates the applicability and accuracy of the LSR method and the CAEH method in determining the CI for Beishan granite, marble, cyan sandstone, and red sandstone. The relationships between porosity and the CI/UCS ratios are investigated for these different types of rocks. The possibility of characterizing crack evolution by residual strain from cyclic loading tests is explored. And the mechanism and engineering significance of the two crack initiation thresholds of Beishan granite are discussed.

Testing methods and data analysis method

Description of rock specimens

The four kinds of rock samples used in the tests were all collected from near the surface. The Beishan granite was from China's first underground research laboratory site. All the specimens for the different rock types are obtained by drilling in the same direction. As shown in Fig. 1, the rock blocks were machined into standard cylindrical specimens ($\Phi 50 \text{ mm} \times 100 \text{ mm}$). The number of specimens used for monotonic loading tests and cyclic loading tests is 12 and 7, respectively. Detailed information is listed in Table 1. The Beishan granite involved in this paper has a relatively high porosity. The reason for the high porosity may be that the samples were collected near the surface, and the electron micrographs showed some pre-existing cracks in the rock.

Testing equipment

An MTS 815.03 electro-hydraulic servo-controlled rock mechanics testing system and an AE acquisition system (MICRO-II-32, from American Physical Acoustics Corporation) were used to coordinately work with each other, as shown in Fig. 2. The operating frequency of the AE acquisition system is 1–400 kHz. During the tests, the AE acquisition system and the mechanical testing system were synchronized. Two sensors were symmetrically arranged on the upper and lower ends of the sample. A proper amount of coupling agent was applied between the sensor and the sample, and the probe was firmly fixed on the specimen with a rubber band. AE signals were recorded with a processing system using a gain of 100 dB and a trigger amplitude threshold of 45 dB.

Loading methods

Two loading methods were used for the work described in this paper: (1) in the monotonic loading tests, axial displacement was used to control the loading. The axial displacement rate

Fig. 1 Test samples of four kinds of rocks before the tests



was 10^{-3} mm/s, and the loading was continuously applied until the samples failed; (2) in the increasing amplitude cyclic stressing tests, samples were first loaded to a certain stress level such as 10 MPa at a controlled axial force of 0.369 kN/s and then unloaded at the same rate to 1 MPa. In each subsequent cycle, the maximum stress was increased by 3–10 MPa and the stress again unloaded to 1 MPa. Stress cycling was continued in this way until samples failed. In the last cycle, the same axial displacement control was taken as that of the monotonic loading test, and the axial displacement rate then was 10^{-3} mm/s. In particular, the increment of axial force was decreased near the estimated CI. Figure 3 shows an example of a loading path for a sample that failed on the 18th loading cycle.

Improved moving point regression technique

Eberhardt et al. (1998) proposed the moving point regression technique in order to better detect the key inflection points on the stress-strain curve. This technique employs a window that can be moved through an x and y data set, and the slope is fitted by linear regression in this window with a user-defined interval. Chen et al. (2016) demonstrated that the fluctuation of the average stiffness curve could be reduced, and the CI could be better identified by taking 10% of the total data as the regression interval in the moving point regression. Although the number of data points in the regression interval is fixed, the stress over the regression interval is variable. The regression interval

Table 1 Basic information about the rock specimens

Rock type	Origin	Mineral composition	Grain size Porosity	Number of tests	
				Monotonic loading tests	Cyclic loading tests
Beishan granite (medium-grained biotite granodiorite)	Gansu, China Block dry density: 2.630 g/cm ³	Albite: 56% Quartz: 19% Microcline: 16% Biotite: 9%	1–5 mm 2.79%	3	4
Marble (medium-grained marble)	Sichuan, China Block dry density: 2.705 g/cm ³	Calcite: 99% Quartz: 1%	1–4 mm 0.86%	3	1
Cyan sandstone (medium-grained feldspar sandstone)	Henan, China Block dry density: 2.385 g/cm ³	Albite: 44% Quartz: 37% Microcline: 9% Illite: 5% Chlorite: 4% Calcite: 1%	0.25–0.5 mm 9.89%	3	1
Red sandstone (medium-grained feldspar sandstone)	Henan, China Block dry density: 2.345 g/cm ³	Quartz: 68% Microcline: 14% Albite: 13% Illite: 3% Kaolinite: 2%	0.25–0.5 mm 11.70%	3	1

Fig. 2 Mechanical testing system and AE acquisition system



of fixed stress size and the moving distance of fixed stress size were implemented by MATLAB (Fig. 4). The regression interval can be user-defined. The larger the regression interval, the smoother the stiffness curve will be, but some key inflection points might be hidden if the range of the regression interval is too large. The recommended regression interval is in the range of 1–10 MPa. More uniform average stiffness on the whole stress-strain curve can be obtained by the improved moving point regression technique, which effectively facilitates the ability of the moving point regression to identify the key inflection points. Moreover, the obtained slope corresponds to the upper bound stress of regression interval, which can reflect the initial stress of the slope variation.

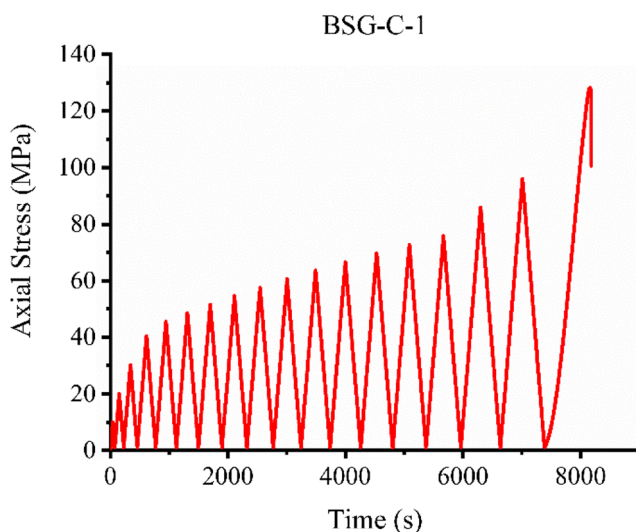


Fig. 3 Example of a loading path from a cyclic loading test on a Beishan granite sample. In the last cycle, axial displacement control was adopted

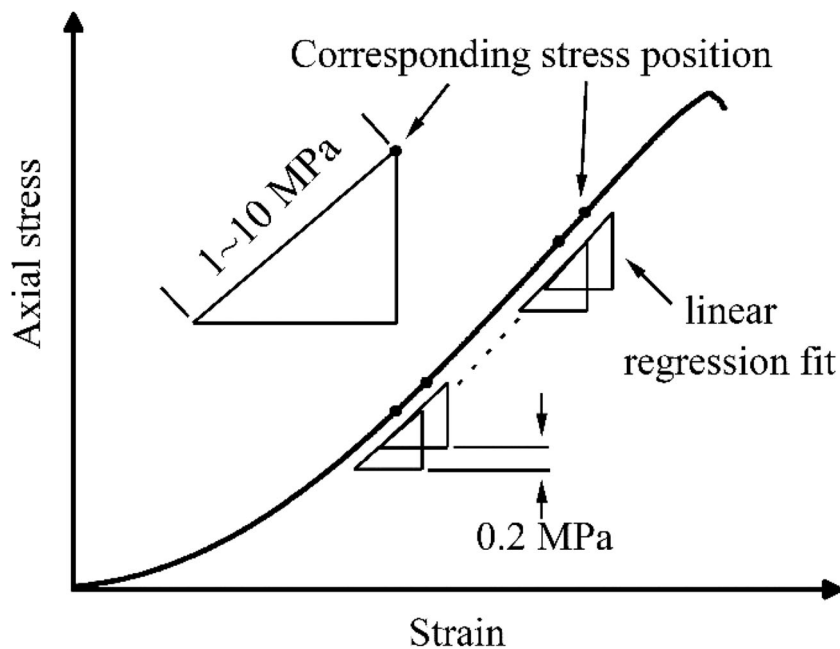
Evaluation of methods for identifying the crack initiation stress of rocks with different porosities

In the uniaxial compression test, the microcracks in the sample propagate along the axial direction (Eberhardt et al. 1998). The strength of the specimen does not degrade during the stable crack propagation stage, and the axial stress-strain curve remains linear at this stage (Lajtai 1974). Therefore, the axial cracks generated by the tensile stress only cause a lateral expansion of the specimen, which is captured by the circumferential strain gauge. The AE equipment records the acoustic signals released by crack initiation and propagation and hence can monitor the real-time damage evolution inside the sample. Therefore, among the existing methods of determining the CI, the method based on stress-lateral strain data and AE data exhibits direct physical meaning. Axial stress-strain data and elastic constants (E , ν) were introduced into the volumetric strain method (Brace et al. 1966), the instantaneous Poisson's ratio method (Diederichs 2007), and the crack volumetric strain (CVS) method (Martin and Chandler, 1994) and may affect the accuracy of the obtained results.

Lateral strain method and lateral strain response method

In the compression tests, the initiation of tensile microcracks inside the sample was reflected in the deviation of the lateral strain curve from linearity. When the lateral strain response exhibited good linear characteristics in the elastic stage, the most direct and effective method to determine CI is by examining the inflection point where the lateral strain curve deviates from linearity.

Fig. 4 Improved moving point regression technique



In Fig. 5, it is very difficult to directly determine the inflection point of the lateral strain curve deviating from linearity for the four kinds of rocks included in this paper. The key inflection point of the lateral strain curve can be found conveniently from the lateral stiffness curve obtained by the improved

moving point regression technique. This method, which uses the improved moving point regression technique to examine the lateral strain stiffness to determine the CI, is called the lateral strain (LS) method, and the CI thus obtained is abbreviated as CI_{LS} . The regression interval for Beishan granite and

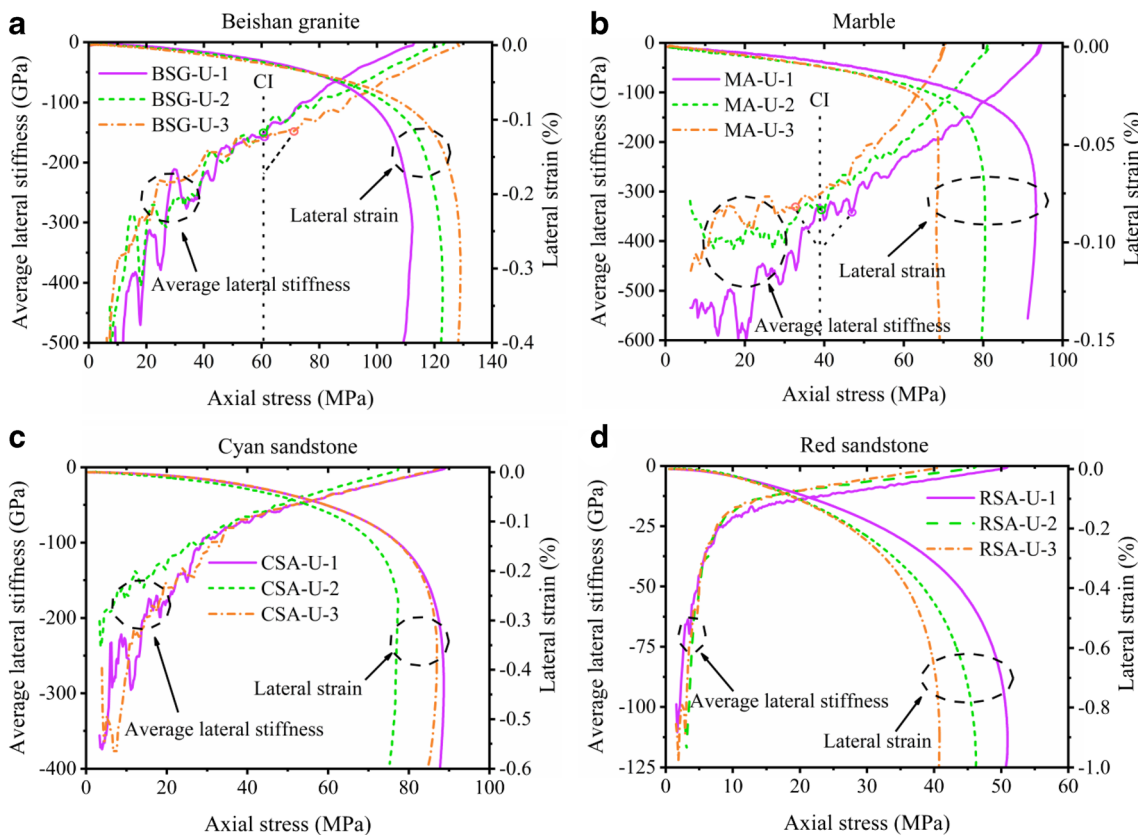


Fig. 5 Plots of lateral strain and lateral stiffness against axial stress for four different porosity rocks

for marble was 7 MPa and that for cyan sandstone and red sandstone was 3 MPa and 1 MPa, respectively. The average CI_{LS} values of Beishan granite and marble were 64.09 MPa and 39.88 MPa, respectively, and their average CI/UCS values were 0.53 and 0.49, respectively. For sandstone with high porosity, there was no real linear stage in the lateral strain curve. The lateral stiffness fluctuation was more obvious during the loading of Beishan granite and marble, which illustrated that these samples experienced stages of obvious energy accumulation and release.

The lateral strain response (LSR) method was proposed by Nicksiar and Martin (2012) to determine the CI. Taking the straight line between the crack damage stress and zero stress as the reference line, the difference between the lateral strain and the reference line (Δ LSR) was calculated. The stress corresponding to the maximum Δ LSR is the CI_{LSR} , as shown in Fig. 6. The crack damage stress (CD_{VS}) herein was obtained by determining the inflection point of the volumetric strain. It can be seen from Fig. 6 that an accurate CI could be obtained by LSR method.

For Beishan granite and marble, the average values of CI_{LSR} were 56.36 MPa and 42.90 MPa, and the average values of CI/UCS were 0.47 and 0.53, respectively. Compared with the LS method, the average CI values obtained by the LSR method were satisfactory, but the results may include certain errors such as in samples BSG-U-3 and MA-U-2 (Table 2). Furthermore, larger standard deviations are found for the results obtained by the LSR method. For sandstone with high porosity, the accuracy of LSR method remains to be verified.

Cumulative AE hits method

AE signals are generated during the initiation and propagation of microcracks. Eberhardt et al. (1998) determined the CI of Lac du Bonnet granite in uniaxial compression by using real-

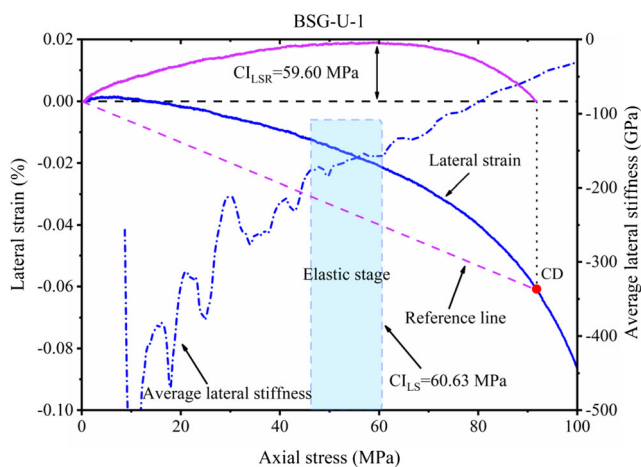


Fig. 6 The crack initiation stress determined by the lateral strain response method

time AE events and ringing counts. Zhao et al. (2013) proposed that the CI could be determined more accurately by identifying the inflection point where the cumulative AE hits curve deviates from linearity. After that, Zhao et al. (2015) put forward the cumulative AE hits (CAEH) method. The AE technique can be used as an alternative method to determine the CI when there is no obvious linear behavior of the lateral strain.

The CAEH method is similar to the LSR method. The key inflection point on the target curve is detected by calculating the difference between the reference line and the curve. The stress corresponding to the maximum difference is the CI_{CAEH} . In the initial stage of loading, the rock was in the crack closure stage, and a lot of AE hits are generated. With the closure of internal flaws, the rock entered the elastic stage, and the AE activity entered a relatively stable period. In this period, the cumulative AE hits curve was characterized by approximate linearity. The cracks began to systematically initiate and propagate with a further increase of load, the AE activity increased, and the inflection point could be observed in the cumulative AE hits curve. Therefore, the CAEH method possesses a clear theoretical basis. For Beishan granite, the results obtained by the CAEH method are in good agreement with those obtained by the LSR method.

The establishment of the reference line of the CAEH method is as follows: first, a tangent line is drawn to the curve of high stress area from the position of the curve close to the zero point; second, a tangent line is drawn from the tangent point obtained in the first step to the curve of low stress area (Fig. 7). The described two tangent points are the upper and lower bounds of the reference line of the CAEH method, respectively. As can be seen from Fig. 7, the establishment of the reference line heavily depends on the “S-shaped” characteristic of the cumulative AE hits curve. It is difficult to establish an effective reference line for the cumulative AE hits curve without the “S-shaped” characteristic. However, the inflection point of the cumulative AE hits curve after crack initiation is indeed real. Next, the slope variation of the cumulative AE hits curve was checked by the improved moving point regression technique.

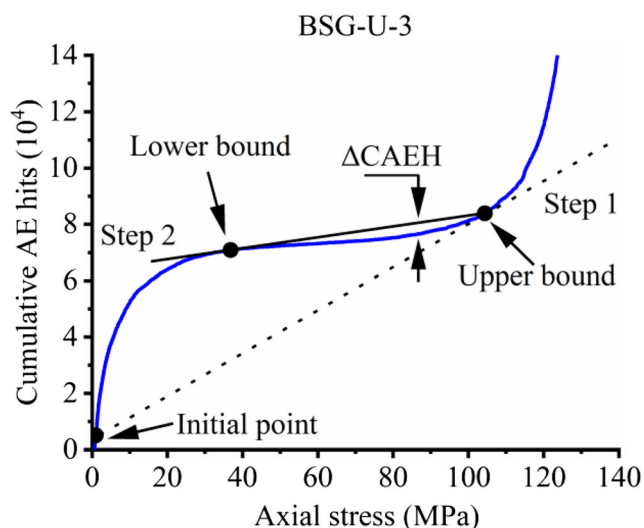
Shown in Fig. 8 are the cumulative AE hits curves and their slope curves for the four types of rocks. The key inflection point where the cumulative AE hits curve deviates from linearity can be easily determined by the variation of the slope curve. The above introduced method is called the cumulative AE hits curve slope (CAHS) method, and the obtained result is abbreviated as CI_{CAHS} . For Beishan granite, the slope of the cumulative AE hits curve began to increase obviously at about 52.40 MPa. This indicated that the cracks began to increase systematically at this stress level, which was obviously smaller than CI_{LS} . However, these initial new cracks did not lead to an obvious expansion of the lateral strain, and they were only detected by AE. It seems that there are two crack initiation

Table 2 Results from lateral strain (LS) method and lateral strain response (LSR) method for determining the CI of Beishan granite and marble

Sample no.	UCS (MPa)	CC/UCS	CD _{VS} /UCS	CI _{LS} /UCS	CI _{LSR} /UCS
BSG-U-1	112.28	0.29	0.82	0.54	0.53
BSG-U-2	122.80	0.28	0.84	0.49	0.50
BSG-U-3	129.05	0.30	0.70	0.55	0.37
Mean	121.38	0.29	0.78	0.53	0.47
SD	6.92	0.01	0.06	0.03	0.07
MA-U-1	93.29	0.22	0.82	0.50	0.50
MA-U-2	80.49	0.21	0.83	0.49	0.58
MA-U-3	69.03	0.29	0.83	0.48	0.52
Mean	80.94	0.24	0.83	0.49	0.53
SD	9.91	0.04	0.00	0.01	0.03

stress thresholds in Beishan granite, 0.43 UCS and 0.53 UCS, respectively (Eberhardt et al. 1999). For marble, the starting point of the systematic increase of cracks can be directly identified by the cumulative AE hits curve. The stresses corresponding to these starting points were very consistent with CI_{LS}. The cumulative AE hits curve of marble showed a temporary surge at about 30.51 MPa. This may mean the initiation of isolated cracks in low strength areas. For the two kinds of sandstones, relatively objective CI_{CAHS} can still be determined according to the slope curve.

In Fig. 9, the uniaxial compressive strength of four different rock specimens and the CI determined by different methods are summarized. When the lateral strain was linear in the elastic stage, the CI could be simply and conveniently determined by the LS method. Compared with the LS method, the results obtained by the LSR method are satisfactory for Beishan granite and marble. The CAEH method has obvious physical significance, but the establishment of its reference line depended heavily on the “S-shaped” characteristic of cumulative AE hits

**Fig. 7** Schematic diagram of the CAEH method

curves, which limits the further application of the CAEH method. The CAHS method possesses the widest applicability and the highest accuracy, and the CI_{CAHS} can be used as the lower limit of the crack initiation stress. A summary of the existing methods is listed in Table 3.

For sandstones with high porosity, although a unique CI value could be obtained by the LSR method, it was obviously smaller than that obtained by the CAHS method. And the higher the porosity, the greater the error. For a small number of samples, manual determination is beneficial to reduce the error as compared with the methods assisted by a reference line. In view of the widest applicability of the LSR method and the CAHS method, the relationship between the results obtained by these two methods and the porosity is plotted in Fig. 10. The porosity of marble (MA), Beishan granite (BSG), cyan sandstone (CSA), and red sandstone (RSA) are 0.86%, 2.79%, 9.89%, and 11.7%, respectively. The four kinds of rocks are divided into two groups: the first group is marble and Beishan granite with low porosity and mineral grain size ranging from 1 to 5 mm; the second group is cyan sandstone and red sandstone with large porosity and mineral grain size ranging from 0.25 to 0.5 mm. It can be concluded from Fig. 10 that in the same group, the normalized CI values obtained by the two methods decrease with the increase of porosity. For rocks with similar structure and texture, higher porosity means more flaws and longer pre-existing cracks (Hatzor and Palchik 1997). These flaws can act as seeds for new cracks and increase the heterogeneity of the stress distribution of the stressed rock, which promotes the initiation and propagation of cracks under lower stress levels (Diederichs 2007). Although the porosity of cyan sandstone is higher than that of marble and Beishan granite, its higher CI/UCS ratios were obtained by the CAHS method. This indicates that the CI/UCS ratio is not only related to porosity but also to mineral composition, grain size, and contact

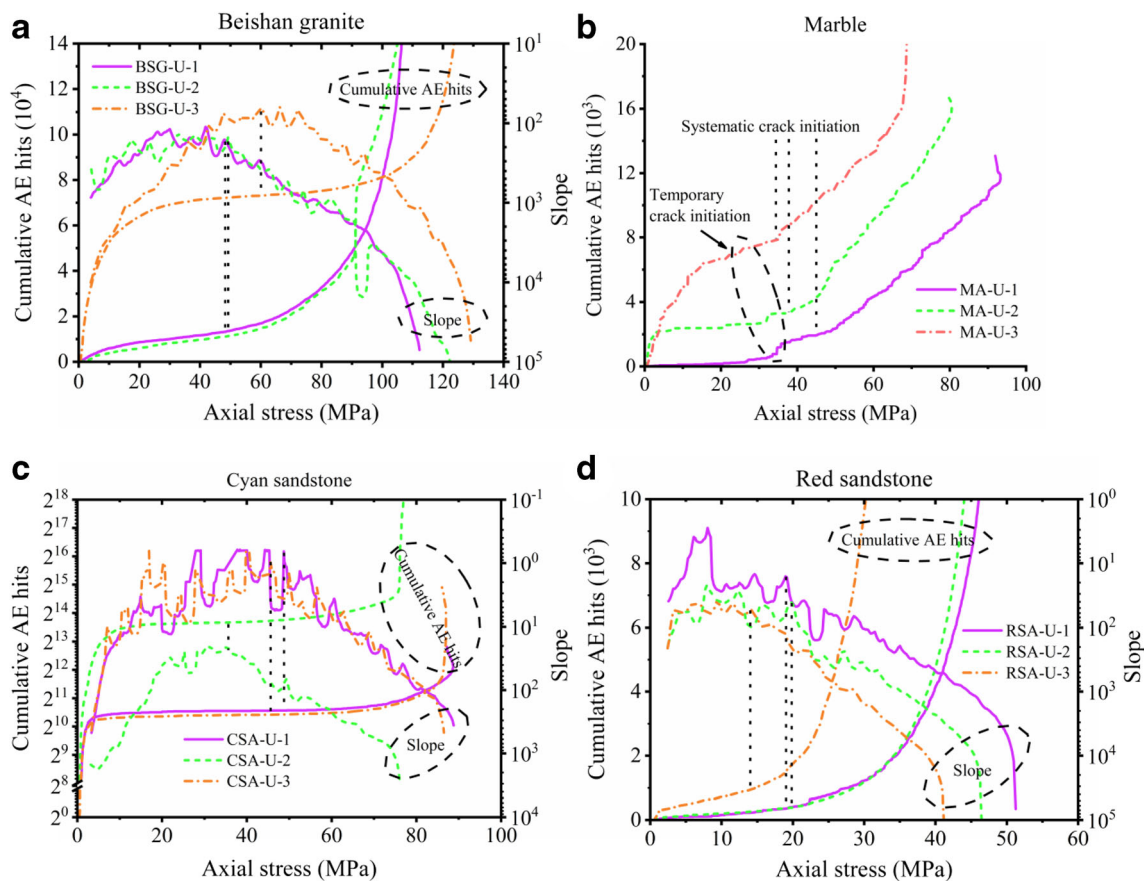


Fig. 8 The key inflection point of cumulative AE hits curve was determined by its slope curve. The stress corresponding to the black-dotted line connecting the two curves is CI_{CAHS}

surface between minerals (Moore and Lockner 1995, Seo et al. 2002).

For the samples with the same lithology, when the load exceeds the CI, the samples with faster lateral stiffness reduction and faster cumulative AE hits curve growth possessed lower peak strength. Compared with other samples, the internal structure of these samples might facilitate the crack initiation and propagation. They exhibited the same mechanism as the degradation of the strength of the rock around deep tunnels, that is, the accumulation of more cracks will reduce the strength of the rock.

Exploration of increasing amplitude cyclic stressing tests to determine the CI

In previous publications, the increasing amplitude cyclic stressing tests were mainly used to analyze the degradation of Young's modulus of the rock (Heap and Faulkner 2008; Heap et al. 2009). During loading, plastic deformation would be produced during the crack closure, as well as the adjustment of mineral particles, and the initiation and propagation of cracks. The increasing amplitude cyclic stressing test is a

novel method to determine the CI by analyzing the variation of plastic strain at different stress level.

Real-time acoustic emission

During loading, a small number of AE signals are generated during the crack closure stage and the elastic deformation stage. As the load increases, energy accumulates in the specimen. When the load reaches the crack initiation threshold, a large number of AE signals suddenly appear. They are accompanied by energy release. Then the cracks enter a stable expansion stage, during which the AE signals are relatively reduced. After the crack closure stress, the relatively isolated peak of the real-time AE hits count indicates the initiation of the cracks. The stress corresponding to this peak is regarded as the crack initiation stress (CI_{AEHC}). In the cyclic loading test, for the four Beishan granite samples, the CI_{AEHC} can be clearly identified and is very close to the CI_{LS} obtained in the monotonic loading test (Fig. 11). Compared with the CI_{CAHS} obtained from the monotonic loading test, the crack initiation and propagation are more severe at the stress level of CI_{AEHC} or CI_{LS} . In these four granite samples, there were obviously more AE activities in samples BSG-C-2 and BSG-C-4 with lower strength. For marble and red sandstone samples, the

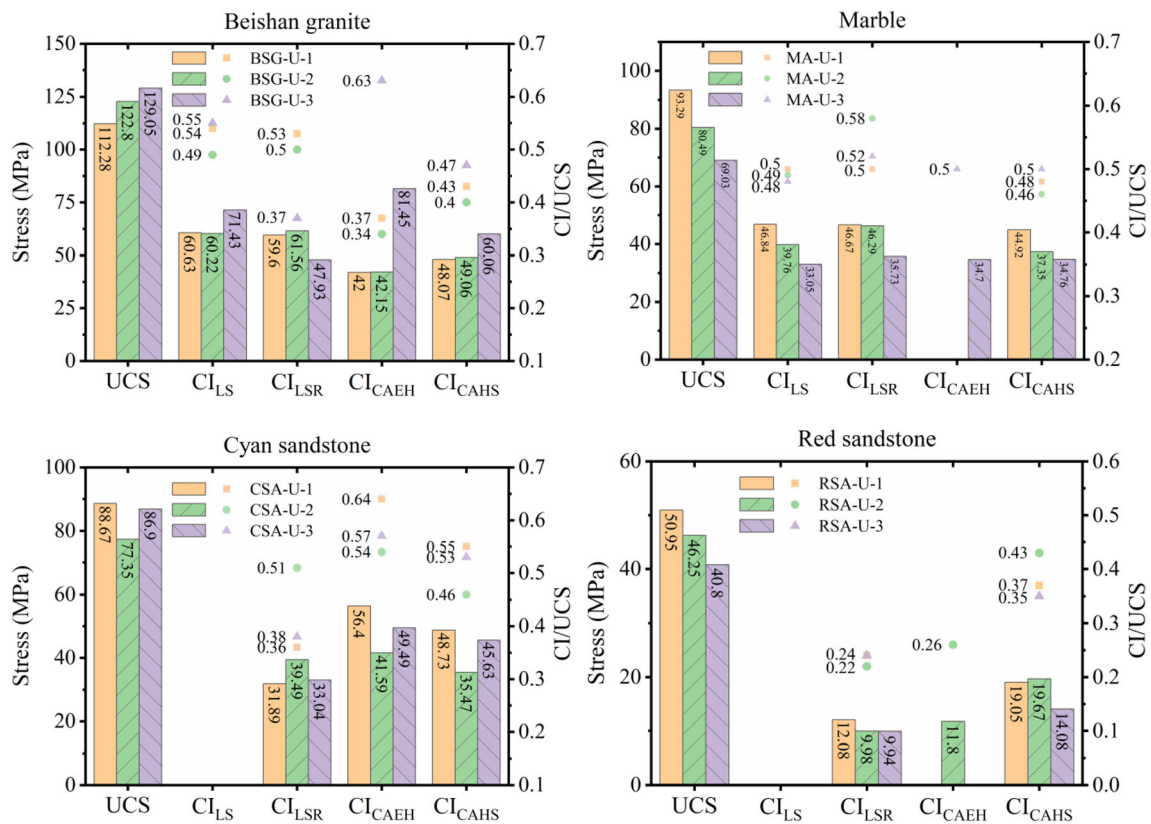


Fig. 9 The UCS of different rocks and the CI obtained by four different methods

CI_{AEHC} obtained were very consistent with the CI_{CAHS} obtained from the monotonic loading tests (Fig. 12a, c). However, the recognition of the sudden increase in real-time AE hits count is subjective to some extent, and it even cannot be accurately identified for cyan sandstone (Fig. 12b).

Residual strain analysis

Figure 13 shows the variation of lateral and axial residual strains at different stress levels for four granite specimens. The lateral residual strain can be divided into three

Table 3 Evaluation of existing methods for determining crack initiation

Existing methods		Advantage	Disadvantage	Note
Based on stress strain data	Volumetric strain method	Simple and easy to use	The result is uncertain	Axial strain data and elastic parameters are introduced into these methods
	Instantaneous Poisson's ratio method			
	Crack volumetric strain method			
Based on AE data	Lateral strain (LS) method	Simple and easy to use	Not suitable for rocks with no linear characteristics of lateral strain	Suitable for Beishan granite and marble studied in this paper
	Lateral strain response (LSR) method	Unique result	The result has a certain error, and the result is too small for high porosity sandstone	The dispersion of the results can be reduced by narrowing the range of the reference line
	Cumulative AE hits (CAEH) method	Unique result	The scope of use is limited	Similar to LSR method
	Cumulative AE hits curve slope (CAHS) method	Wide application range, accurate results	Somewhat subjective	Very sensitive to crack initiation

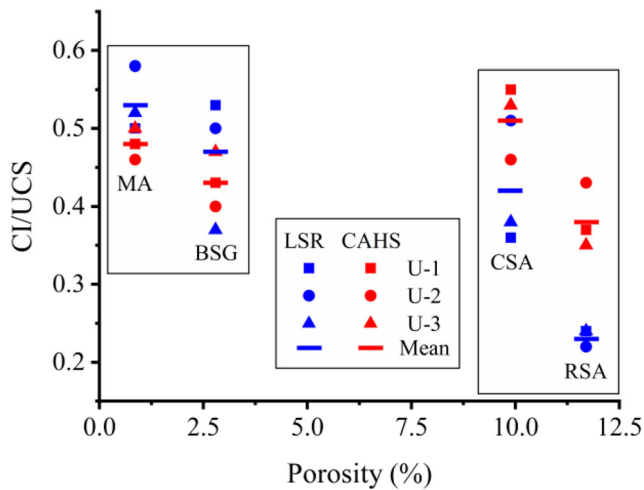


Fig. 10 Relations of normalized CI against porosity in different rocks. The blue and red symbols represent the results obtained by the LSR method and the CAHS method, respectively

characteristic stages: in stage I, the residual strain is basically stable; in stage II, the residual strain increases slowly; and in stage III, the residual strain increases rapidly. This indicates that in granite, two crack initiation thresholds can be determined by lateral residual strain. The lower limit of stage II

corresponds to the first crack initiation (CI_{RS1}), and the lower limit of stage III corresponds to the second crack initiation (CI_{RS2}). The two stress levels are approximately equal, respectively, to CI_{CAHS} and CI_{LS} in the monotonic loading test of Beishan granite. The axial residual strain exhibits three different characteristics in the above mentioned three stages: stage I can be divided into two parts. Before the loading to 10 MPa, the primary flaws in the sample were closed rapidly, resulting in a large plastic deformation. After the loading beyond 10 MPa, the axial plastic deformation maintained stable growth; in stage II, the increase of axial residual strain tended to slow down; in stage III, the increase of axial residual strain further slowed down. In these three stages, the slope of the stress axial residual strain curve seemed to decrease in a regular manner, which is an interesting phenomenon.

The variation of lateral and axial residual strain reflects the evolution of plastic deformation at different stages at the macro scale. In stage I, the lateral residual strain remained unchanged, while the axial residual strain continued to increase, indicating that the plastic strain in this stage mainly came from the axial compaction of flaws and the axial adjustment of mineral particles. When the stress level exceeds CI_{RS1} , the cracks began to initiate systematically. At this time, the cracks

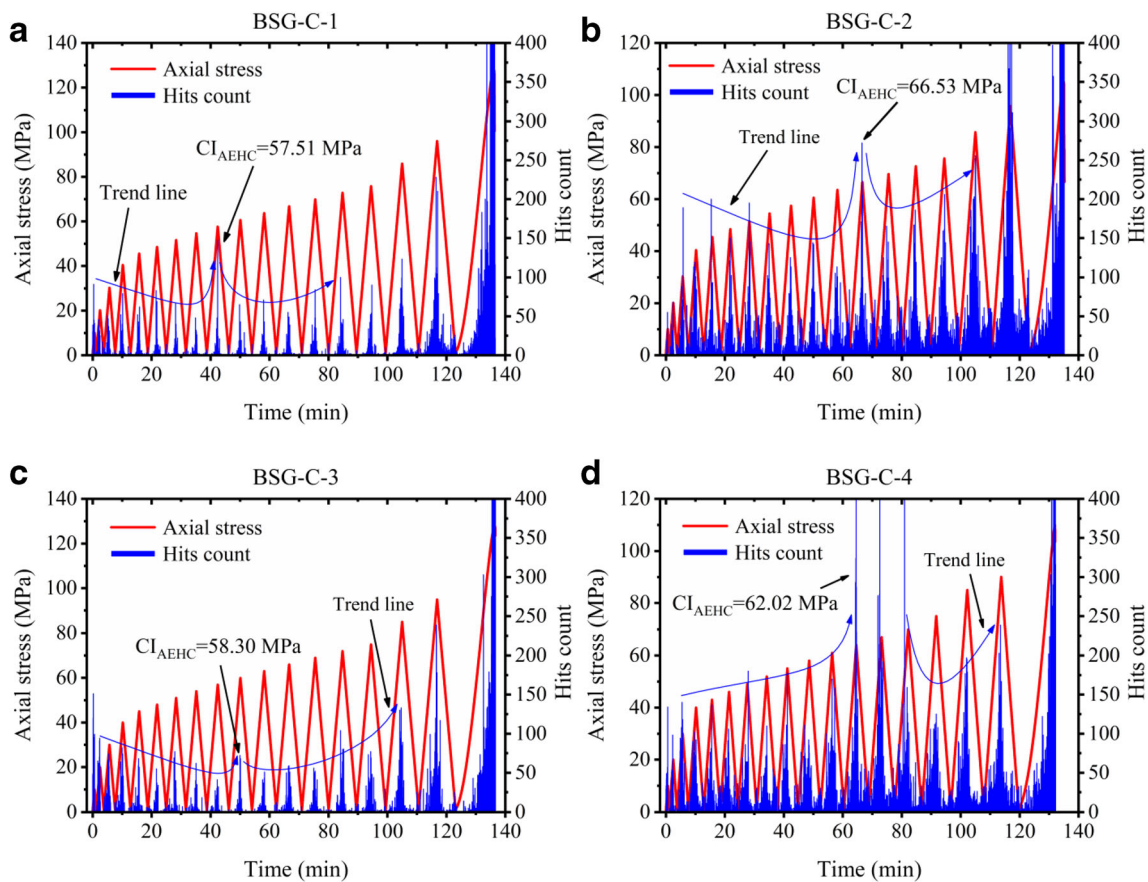


Fig. 11 Output of acoustic hits count, as a function of stress and time, from cyclic loading tests on four samples of Beishan granite. The blue arrows represent the trend lines of the AE hits count

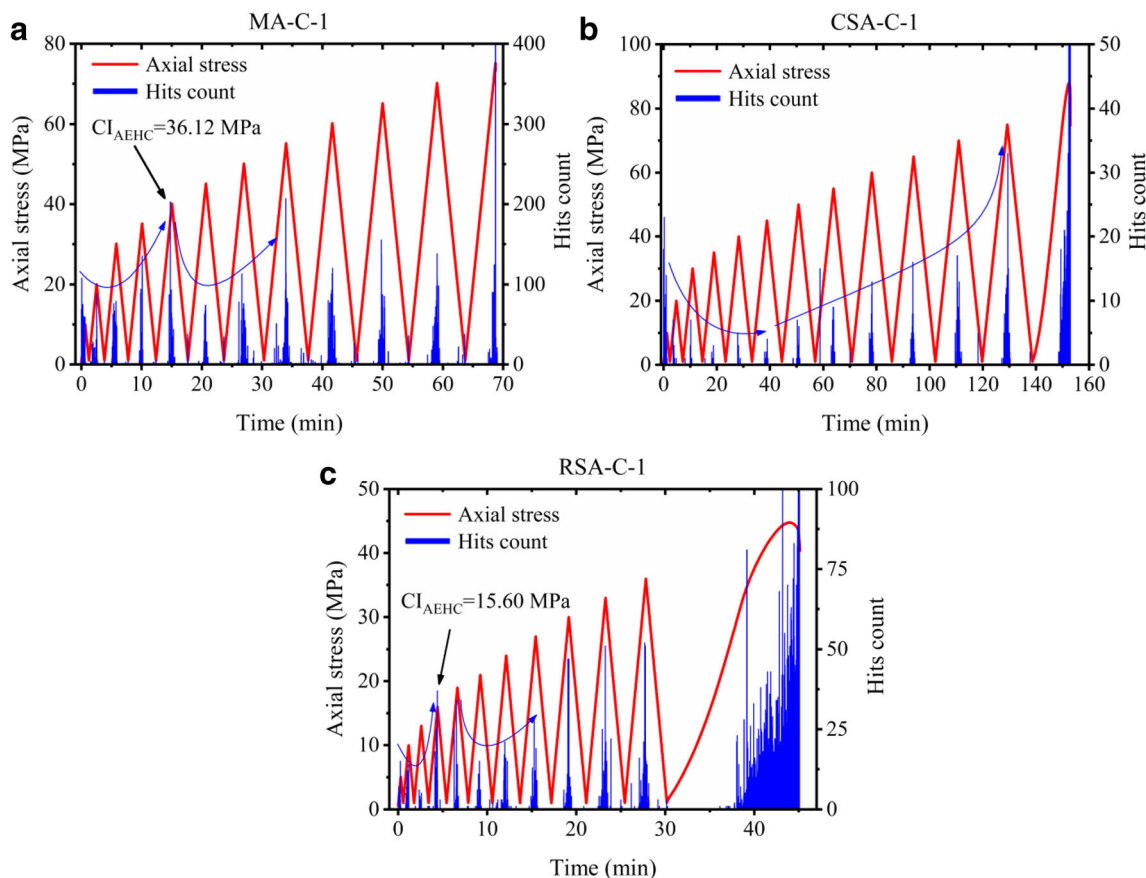


Fig. 12 Output of acoustic hits count, as a function of stress and time, from cyclic loading tests on marble, red sandstone, and cyan sandstone. The blue arrows represent the trend lines of the AE hits count

mainly propagated along the mineral boundary and weak planes of minerals that have low elastic modulus (Akesson et al. 2004, Chen et al. 2011, Ghasemi et al. 2020), accompanied by a small increase in the number of AE hits, which is reflected in the deviation from linearity of the cumulative AE hits curve. The obvious degradation of lateral stiffness was not induced by these small numbers of cracks. When the stress level exceeds CI_{RS2} , the real-time AE hits count showed a

relatively isolated peak, and the lateral stiffness began to decrease obviously. This indicated that axial cracks have formed in the quartz (Eberhardt et al. 1999, Heap and Faulkner 2008, Chen et al. 2011, Basu et al. 2013, Ghasemi et al. 2020). The Beishan granite sample after the test showed typical splitting failure (Fig. 14).

Renshaw and Schulson (2001) proposed that a stress concentration occurs at the end of the sliding section due to the

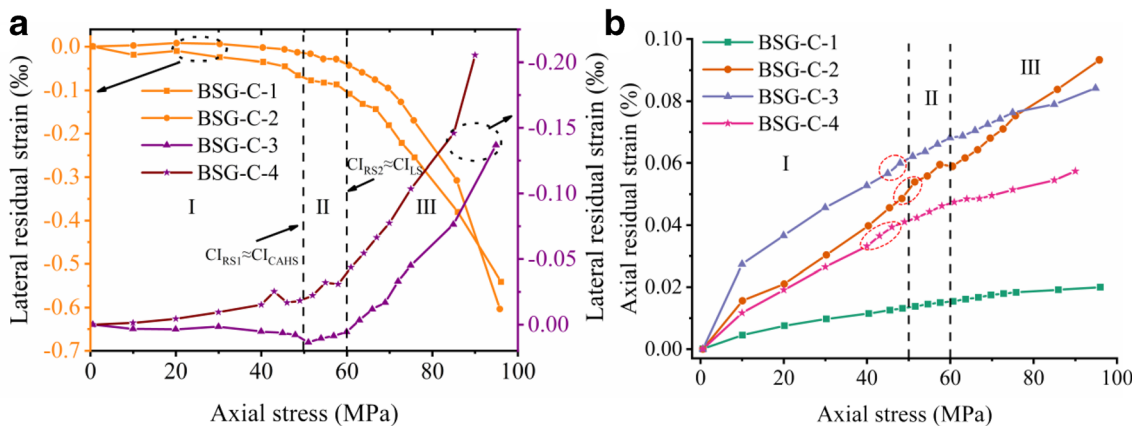
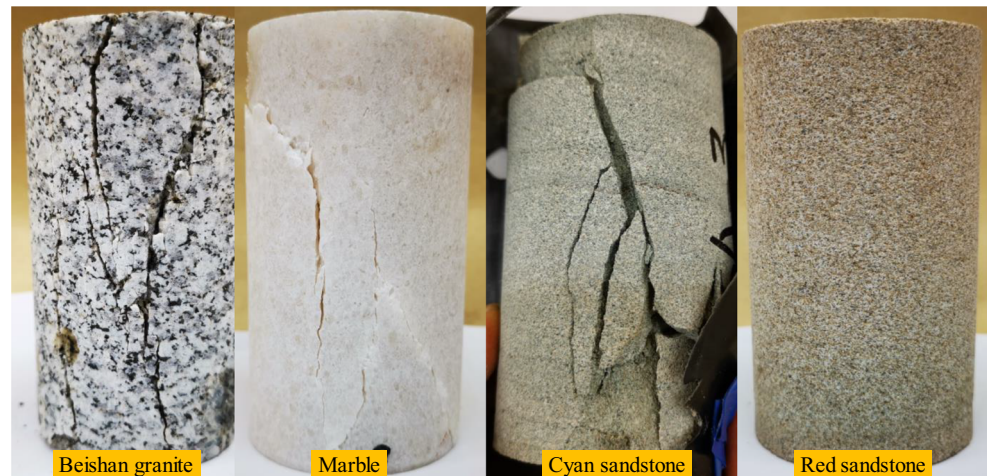


Fig. 13 The residual strain of four granite samples after unloading at different stress levels. **a** Lateral residual strain; **b** axial residual strain. In order to show the results clearly, two different scales were used in the lateral residual strain

Fig. 14 Photographs of samples after uniaxial compression tests



sliding along the primary cracks, which causes the stress around the tip of the sliding section to exceed the yield stress of the material, resulting in the initiation of secondary cracks. It can be seen from the section circled by the red curve in Fig. 13b that the axial residual strain increased transiently before the crack initiation, indicating that the pre-existing cracks in the sample have slipped. After that, the lateral residual strain began to increase slowly, and the secondary cracks began to initiate (Fig. 13a). This illustrated that in Beishan granite, one part of the first crack initiation was caused by the sliding of the primary cracks. Interestingly, the lateral residual strain increased, while the increase of axial residual strain slowed down during the stages II and III. Furthermore, with the increase of stress, the increment of axial residual strain slowed down more obviously (Fig. 13b). This may mean that as the stress increases in granite, tensile cracks gradually dominate. The mineral particles between adjacent tensile cracks are arranged more closely, which inhibits their axial adjustment. The inhibition effect lasts until cracks coalescence, at which point the axial stiffness begins to degrade. The above assumption can be well verified on the average axial stiffness curve under uniaxial compression (Fig. 15). When the stress entered stage II, the average axial stiffness curves of BSG-U-1 and BSG-U-2 showed an obvious inflection point, which represented the reduction of axial deformation. In stage III, the axial plastic deformation was further restrained by the directional increase of intragranular cracks, and the axial stiffness tended to remain stable. This phenomenon fully demonstrated that the newly initiated cracks had the ability to restrain the axial deformation. For the Beishan granites obtained from near the surface, the maximum axial stiffness appeared during the stage of stable crack propagation rather than during the elastic stage. This also demonstrated that the results obtained by the method of introducing axial strain data to determine the CI possessed uncertainty.

The residual strain of marble can also be divided into three stages (Fig. 16a). In the stage II, the lateral and axial residual

strain increased suddenly and continuously, and the increase of axial residual strain did not slow down. This demonstrated that in this stage, stable shear cracks initiate on the grain boundary or cleavage plane. The threshold (CI_{AEHC}) at which the cracks started in the calcite was in stage II, but these cracks did not cause significant changes in the residual strain. This may be because marble has a unique microcrack nucleation mechanism—gliding along twin lamellae (Chen et al. 2016). In stage III, the lateral and axial residual strain increased significantly, and the increase of lateral residual strain was faster, illustrating that the initiation and propagation of cracks are more active. In addition, the tensile cracks and shear cracks were both accelerating and accumulating, especially the tensile cracks. Different from Beishan granite, the marble showed the accumulation of shear cracks in stage II and stage III, and

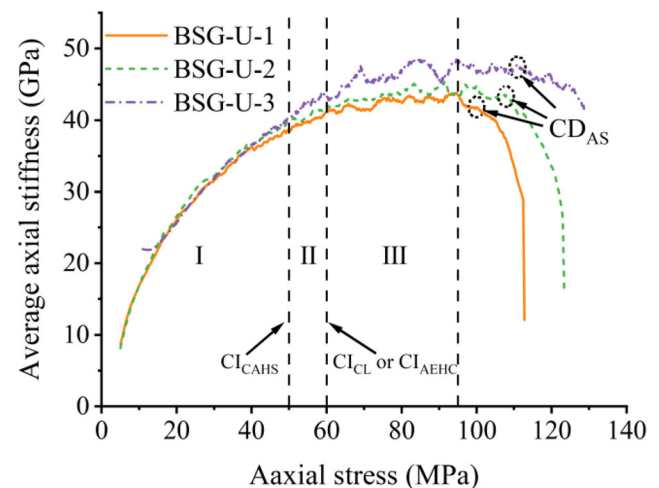


Fig. 15 The average axial stiffness curves of three Beishan granite samples under uniaxial compression were obtained by the improved moving point regression technique. The regression interval was 5 MPa. The stress corresponding to the beginning of the axial stiffness decay is the crack damage stress (CD_{AS}), and the stage III is entirely in the stable crack growth stage

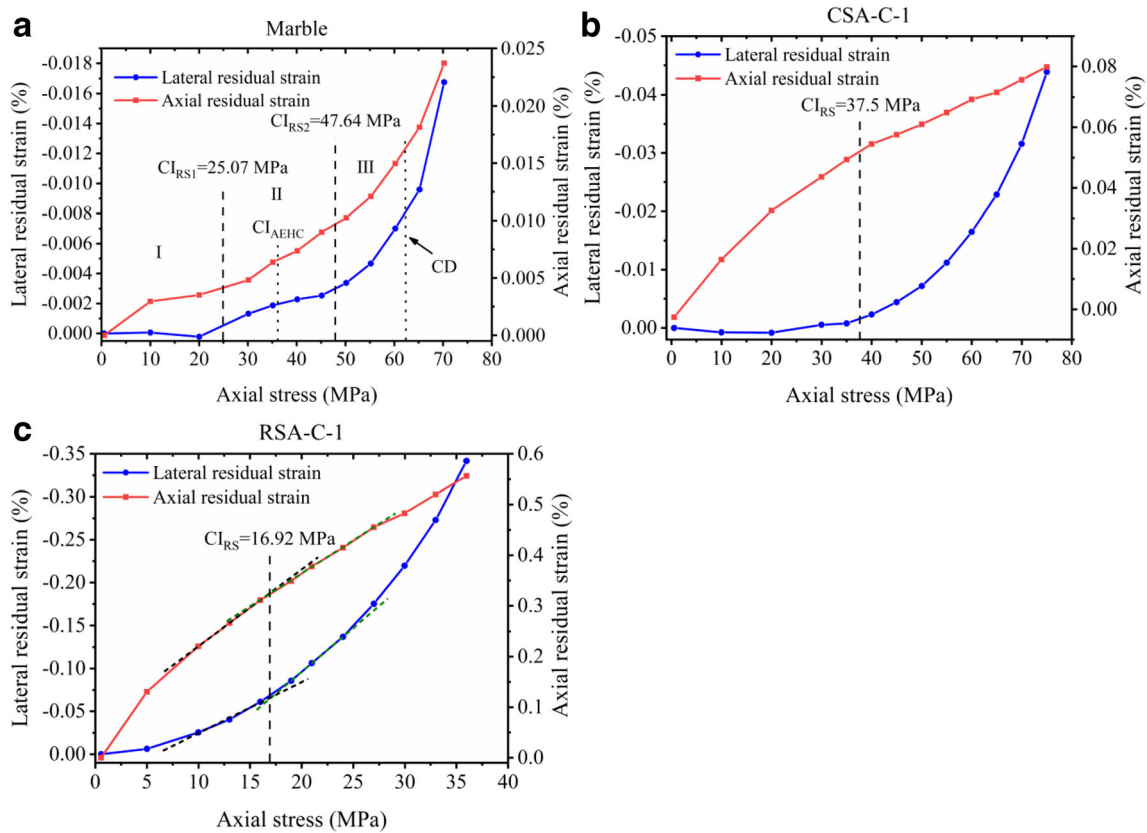


Fig. 16 Residual strain of marble, cyan sandstone, and red sandstone after unloading at different stress levels

this increased rapidly in stage III. This is the reason why the marble samples showed a shear band after failure (Fig. 14).

Although the AE hits count cannot be used to determine the CI_{AEHC} of sample CSA-C-1, a CI_{RS} value close to that of CI_{CAHS} can be determined from the sudden increase of lateral residual strain in Fig. 16b. Similarly, the increase of axial residual strain began to decrease near CI_{RS} and then remained stable. It can be observed in Fig. 17 that the axial stiffness gradually reached the peak after the crack initiation. There was no obvious inflection point in the lateral residual strain curve of red sandstone (Fig. 16c). Two reference lines were added to the convex axial residual strain curve to determine the inflection point where the increment of axial residual strain began to decrease. Two reliable reference lines can also be established on the lateral residual strain curve near the stress level corresponding to the inflection point. It is obvious that the stress corresponding to the intersection point of the reference line is CI_{RS} . In Fig. 14, there are no obvious cracks in the sample after the test because of the large plasticity of red sandstone. Different from Beishan granite and marble, the crack initiation of the two sandstones was not divided into two stages, because the mineral particles in the sandstones are small and any cracks can easily bypass these particles to spread when propagating.

The last cyclic loading cycle in cyclic tests is the same as that in monotonic tests. It can be seen from Table 4 that the

peak strength of the samples in cyclic tests is slightly lower than that in monotonic loading tests, but the difference is small. For Beishan granite, CI_{CAHS} and CI_{LS} (or CI_{LSR}) in monotonic loading tests correspond to CI_{RS1} and CI_{RS2} in cyclic tests, respectively. For marble, CI_{CAHS} and CI_{LSR} in monotonic tests are approximately equal to CI_{RS2} in cyclic tests. The increase of AE hits and lateral strain is not obvious

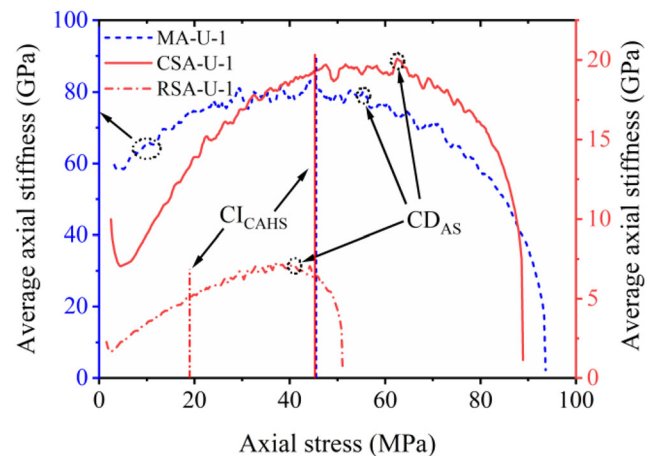


Fig. 17 Typical average axial stiffness curves of marble, cyan sandstone, and red sandstone obtained by improved moving point regression. The stress corresponding to the starting point of axial stiffness degradation was taken as the crack damage stress (CD_{AS})

Table 4 Results of monotonic and cyclic tests for four types of rocks

Stress (MPa)	Uniaxial compression tests			Cyclic tests			
	Peak strength	CI_{LSR}	CI_{CAHS}	Peak strength	CI_{AEHC}	CI_{RS1}	CI_{RS2}
Beishan granite	121.38	56.36	52.40	117.81	61.09	50.73	59.38
Marble	80.94	42.90	39.01	75.18	36.12	25.07	47.50
Cyan sandstone	84.31	34.81	43.28	87.80	\	37.50	
Red sandstone	46.00	10.67	17.60	44.78	15.60	16.92	

at the CI_{RS1} stress level, so the first crack initiation in marble is not observed.

Discussion

Acceptable results could be obtained for Beishan granite and marble with low porosity by the LSR method. Nevertheless, the average CL_{LSR} of cyan sandstone and red sandstone with high porosity is 20% and 39% smaller than the corresponding average CI_{CAHS} , respectively. It can be seen from Fig. 18 that the shape of the lateral stress-strain curves of granite with low

porosity and red sandstone with high porosity is significantly different. In the stage of stable propagation of cracks, the lateral strain of granite increased more obviously, while that of red sandstone did not exhibit prominent variations. This may be due to the high porosity of red sandstone, and that some pores and cracks were not compacted during the stable propagation of cracks. These non-compacted pores and cracks offset part of the plastic deformation generated by crack initiation. Therefore, the lateral stress-strain curve of sandstone had no obvious inflection point near the crack initiation stress, which led to the relatively large error of the LSR method. The higher the porosity, the less obvious the inflection point of the

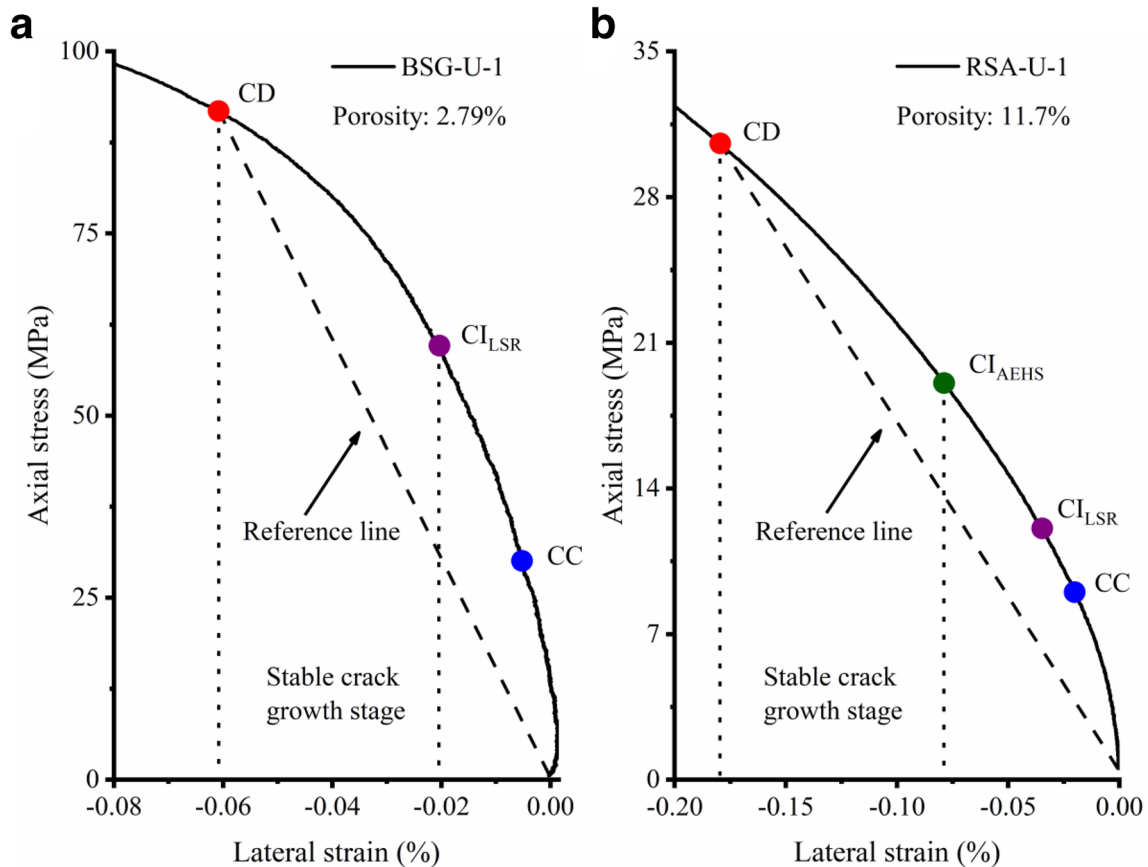


Fig. 18 The relationship between the reference line of the LSR method and the lateral stress-strain curve: (a) Beishan granite; (b) red sandstone

lateral strain near the crack initiation stress would be. The higher the porosity, the more prominent the inflection point of the lateral strain near the crack closure stress, which led to the CI_{LSR} gradually approaching the CC value with the increase of porosity.

In the uniaxial compression tests, for the Beishan granite, the CI_{CAHS} was significantly lower than the CI_{LS} , about 0.43 UCS and 0.53 UCS, respectively. In the cyclic loading tests of granite, the CI_{AEHC} of Beishan granite is about 0.52 UCS, very close to CI_{LS} . This indicated that axial cracks began to appear in some hard minerals (such as quartz) within the sample. The initiation of these cracks not only produced a large number of AE signals but also caused the lateral strain to obviously deviate from the linearity. Ghasemi et al. (2020) observed that the crack initiation sequence was different in the grain boundaries and different types of minerals. They considered this to be the reason for the two crack initiation stress thresholds of granite. In the Mine-by test tunnel, the deviator stress corresponding to the initiation of AE activity and spalling are about 70–75 MPa and 100–120 MPa, respectively (Martin 1997). For the undamaged pink Lac du Bonnet granite, the first and second crack initiation stresses are about 81.5 MPa and 103.9 MPa, respectively (Eberhardt et al. 1999). Martin (1997) reported that the maximum failure depth of the tunnel could be reasonably estimated by the profile with deviator stress of 70–80 MPa in front of the tunnel face. Therefore, it was deduced that the brittle spalling in the granite should meet two conditions at the same time. Firstly, the maximum deviator stress in front of tunnel face exceeded the first crack initiation stress, and the stress direction rotated. In this way, microcracks will fully initiate and propagate at the grain boundaries and weak surfaces (Diederichs et al. 2004). Secondly, when the pre-processed rock mass was located behind the tunnel face, the deviator stress at the excavation boundary exceeded the second crack initiation stress, and the cracks would initiate and propagate in a certain direction in the hard minerals. Subsequently, these cracks coalesced with the previous cracks, resulting in spalling and failure of the rock at the excavation boundary under the relatively low stress. Thus, the relationship between the stress path and the double crack initiation determined the brittle failure of underground tunnels in granite. Li et al. (2021) reported a true-triaxial loading method with variable loading direction, which provides an experimental basis for studying stress rotation. However, this hypothesis needs to be further confirmed by microscopic research and accurate numerical simulation.

Conclusions

In this paper, existing methods for determining the crack initiation stress were evaluated. For brittle rock with low porosity, the lateral strain (LS) method is a very convenient and

effective method to determine the crack initiation stress (CI_{LS}). Compared with the cumulative AE hits (CAEH) method, the cumulative AE hits curve slope (CAHS) method does not rely on the “S-shaped” characteristic of the cumulative AE hits curve and exhibits wider applicability and higher accuracy. Two crack initiation stress thresholds of Beishan granite can be obtained by the CAHS method and LS method, 0.43 UCS and 0.53 UCS, respectively. For high porosity sandstone, the results obtained by LSR method are obviously smaller. Porosity affects the accuracy of the LSR method by affecting the shape of the lateral stress-strain curve.

Using the variation of residual strain to characterize the initiation and propagation of cracks was explored in this paper. It was found that the lateral residual strain was very sensitive to crack initiation, and two crack initiation stress thresholds of Beishan granite and marble can be clearly determined, which indicates that cracks have different initiation sequences in grain boundaries and minerals. It is found that the initiation of cracks can limit the axial plastic deformation of Beishan granite before the cracks coalesce.

The mean values of the CI_{CAHS}/UCS ratio for marble, Beishan granite, cyan sandstone, and red sandstone are 0.48, 0.43, 0.51, and 0.38, respectively. For rocks with similar structure and fabric, the CI/UCS ratios decrease with increasing porosity.

Abbreviations E , Elasticity modulus; ν , Poisson's ratio; AE, Acoustic emission; CC, Crack closure stress; CI, Crack initiation stress; CD, Crack damage stress; UCS, Uniaxial compressive strength; CVS, Crack volumetric strain; LS, Lateral strain; LSR, Lateral strain response; RCSR, Relative compression strain response; CAEH, Cumulative AE hits; CAHS, Cumulative AE hits curve slope; AEHC, AE hits count; RS, Residual strain; AS, Axial stiffness

Acknowledgements The authors are sincerely grateful to Professor Jaak J Daemen, Mackay School of Earth Sciences and Engineering, University of Nevada, for his thoughtful proofreading of this paper.

Funding This work was supported by the Key Projects of the National Natural Science Foundation of China (grant number 51234004), the Project of Decommissioning of Nuclear Facilities and Radioactive Waste Management, and the National Key Research and Development Program of China (NO. 2017YFC0804601, 2018YFC0808403).

Declarations

Conflict of Interest The authors declare no competing interests.

References

- Akesson U, Hansson J, Stigh J (2004) Characterisation of microcracks in the Bohus granite, western Sweden, caused by uniaxial cyclic loading. *Eng Geol* 72(1):131–142
- Andersson C, Martin CD, Stille H (2009) The Äspö pillar stability experiment: part II—rock mass response to coupled excavation-induced

- and thermal-induced stresses. *Int J Rock Mech Min Sci* 46(5):865–878
- Brace WF, Paulding BW Jr, Scholz CH (1966) Dilatancy in the fracture of crystalline rocks. *J Geophys Res* 71(16):3939–3953
- Basu A, Mishra DA (2014) A method for estimating crack-initiation stress of rock materials by porosity. *J Geol Soc India* 84(2014):397–405
- Basu A, Mishra DA, Roychowdhury K (2013) Rock failure modes under uniaxial compression, Brazilian, and point load tests. *Bull Eng Geol Environ* 72:457–475
- Cai M, Kaiser PK, Tasaka Y, Maejima T, Morioka H et al (2004) Generalized crack initiation and crack damage stress thresholds of brittle rock masses near underground excavations. *Int J Rock Mech Min* 41(5):833–847
- Chen SW, Yang CH, Wang GB, Wei X (2016) Experimental study on the determination method of σ_{cc} , σ_{ci} and σ_{cd} for granite under different confining pressures. *J Northeast Univ* 37(12):1789–1793
- Chen Y, Watanabe K, Kusuda H, Kusaka E, Mabuchi M (2011) Crack growth in Westerly granite during a cyclic loading test. *Eng Geol* 117:189–197
- Chen S, Wang G, Zuo S, Yang C (2021) Experimental investigation on microstructure and permeability of thermally treated Beishan granite. *J Test Eval* 49(2)
- Diederichs MS (2007) The 2003 Canadian Geotechnical Colloquium: mechanistic interpretation and practical application of damage and spalling prediction criteria for deep tunnelling. *Can Geotech J* 44(9):1082–1116
- Diederichs MS, Kaiser PK, Eberhardt E (2004) Damage initiation and propagation in hard rock during tunnelling and the influence of near-face stress rotation. *Int J of Rock Mech Min* 41(5):785–812
- Eberhardt E, Stead D, Stimpson B, Read RS (1998) Identifying crack initiation and propagation thresholds in brittle rock. *Can Geotech J* 35(2):222–233
- Eberhardt E, Stead D, Stimpson B (1999) Quantifying progressive prepeak brittle fracture damage in rock during uniaxial compression. *Int J Rock Mech Min Sci* 36:361–380
- Fairhurst C, Cook NGW (1966) The phenomenon of rock splitting parallel to the direction of maximum compression in the neighborhood of a surface. In: *Proceedings of the 1st congress of the international society of rock mechanics*, Lisbon, pp 687–692
- Ghasemi S, Khamsehchiyan M, Taheri A et al (2020) Crack evolution in damage stress thresholds in different minerals of granite rock. *Rock Mech Rock Eng* 53:1163–1178
- Heap MJ, Faulkner DR (2008) Quantifying the evolution of static elastic properties as crystalline rock approaches failure. *Int J Rock Mech Min* 45(4):564–573
- Heap MJ, Vinciguerra S, Meredith PG (2009) The evolution of elastic moduli with increasing crack damage during cyclic stressing of a basalt from Mt. Etna volcano *Tectonophysics* 471(1):153–160
- Hatzor YH, Palchik V (1997) The influence of grain size and porosity on crack initiation stress and critical flaw length in dolomites. *Int J Rock Mech Min Sci* 34(5):805–816
- Lajtai EZ (1974) Brittle fracture in compression. *Int J Fract* 10(4):525–536
- Li L, Hu J, Li S et al (2021) Development of a novel triaxial rock testing method based on biaxial test apparatus and its application. *Rock Mech Rock Eng*
- Martin CD (1997) Seventeen Canadian Geotechnical Colloquium: the effect of cohesion loss and stress path on brittle rock strength. *Can Geotech J* 34:698–725
- Martin CD, Chandler NA (1994) The progressive fracture of Lac du Bonnet granite. *Int J Rock Mech Min Sci Geomech Abstr* 31(6):643–659
- Martin CD, Christiansson R (2009) Estimating the potential for spalling around a deep nuclear waste repository in crystalline rock. *Int J Rock Mech Min Sci* 46:219–228
- Martin CD, Kaiser PK, McCreath DR (1999) Hoek-Brown parameters for predicting the depth of brittle failure around tunnels. *Can Geotech J* 36(1):136–151
- Moore DE, Lockner DA (1995) The role of microcracking in shear-fracture propagation in granite. *J Struct Geol* 17:95–114
- Nicksiar M, Martin CD (2012) Evaluation of methods for determining crack initiation in compression tests on low-porosity rocks. *Rock Mech Rock Eng* 45(4):607–617
- Nicksiar M, Martin CD (2013) Crack initiation stress in low porosity crystalline and sedimentary rocks. *Eng Geol* 154:64–76
- Palchik V, Hatzor YH (2002) Crack damage stress as a composite function of porosity and elastic matrix stiffness in dolomites and limestones. *Eng Geol* 63(3–4):233–245
- Peng J, Rong G, Jiang MY (2018) Variability of crack initiation and crack damage for various rock types. *Arab J Geosci* 11(11):265
- Renshaw C, Schulson E (2001) Universal behaviour in compressive failure of brittle materials. *Nature* 412:897–900
- Seo YS, Jeong GC, Kim JS, Ichikawa Y (2002) Microscopic observation and contact stress analysis of granite under compression. *Eng Geol* 63:259–275
- Taheri A, Zhang Y, Munoz H (2020) Performance of rock crack stress thresholds determination criteria and investigating strength and confining pressure effects. *Constr Build Mater* 243(2020):118263
- Wang J, Chen L, Su R, Zhao XG (2018) The Beishan underground research laboratory for geological disposal of high-level radioactive waste in China: planning, site selection, site characterization and in situ tests. *J Rock Mech Geotech Eng* 10(3):411–435
- Wen T, Tang HM, Ma JW, Wang YK (2018) Evaluation of methods for determining crack initiation stress under compression. *Eng Geol* 235:81–97
- Zhao XG, Cai M, Wang J, Ma LK (2013) Damage stress and acoustic emission characteristics of the Beishan granite. *Int J Rock Mech Min* 64(12):258–269
- Zhao XG, Cai M, Wang J, Li PF, Ma LK (2015) Objective determination of crack initiation stress of brittle rocks under compression using AE measurement. *Rock Mech Rock Eng* 48(6):2473–2484